Development of the error-monitoring system from ages 9-35: unique insight provided by MRI-constrained source localization of EEG

George A. Buzzell[1,*], **John E. Richards**[2], **Lauren K. White**[3], **Tyson V. Barker**[1], **Daniel S. Pine**[4], and **Nathan A. Fox**[1]

[1]Department of Human Development and Quantitative Methodology, University of Maryland, College Park, MD 20742

[2]Department of Psychology, University of South Carolina, Columbia, SC 29208

[3]Department of Child and Adolescent Psychiatry, The Children's Hospital of Philadelphia, Philadelphia, PA 19104

[4]Emotion and Development Branch, Intramural Research Program, National Institute of Mental Health, Bethesda, MD 20814

Abstract

The ability to self-detect errors and dynamically adapt behavior is a cornerstone of higher-level cognition, requiring coordinated activity from a network of neural regions. However, disagreement exists over how the error-monitoring system develops throughout adolescence and early adulthood. The present report leveraged MRI-constrained EEG source localization to detail typical development of the error-monitoring system in a sample of 9–35 year-olds (n=43). Participants performed a flanker task while high-density EEG was recorded; structural MRIs were also acquired for all participants. Analysis of the scalp-recorded EEG data revealed a frontocentral negativity (error-related negativity; ERN) immediately following errors for all participants, although the topography of the ERN varied with age. Source localization of the ERN time range revealed maximal activity within the posterior cingulate cortex (PCC) for all ages, consistent with recent evidence that the PCC provides a substantial contribution to the scalp-recorded ERN. Activity within a network of brain regions, including dorsal anterior cingulate, PCC, and parietal cortex, was predictive of improved performance following errors, regardless of age. However, additional activity within insula, orbitofrontal cortex and inferior frontal gyrus linearly increased with age. Together, these data suggest that the core error-monitoring system is online by early adolescence and remains relatively stable into adulthood. However, additional brain regions become embedded within this core network with age. These results serve as a model of typical development of the error-monitoring system from early adolescence into adulthood.

*Corresponding author: George A. Buzzell, Benjamin Building, 3942 Campus Dr., College Park, MD 20742. gbuzzell@umd.edu.

Keywords

error-monitoring; ERN; source-localization; development; adolescence; posterior cingulate

Achieving goal-directed behavior and maintaining task performance requires the online monitoring of performance in order to detect errors. The neural basis of such error monitoring is observable in scalp-recorded EEG as a fronto-central negativity for error vs. correct responses, termed the error-related negativity (ERN; Falkenstein et al., 1990; Gehring et al., 1993). Studies have demonstrated that ERN magnitude is predictive of immediate error correction (Gehring et al., 1993), as well as improved performance on subsequent trials (Maier et al., 2011), consistent with the notion that error monitoring facilitates task performance. Additionally, an extensive body of research has linked individual differences in error-related processing to psychopathology, extending interest in error monitoring into the clinical domain (see Olvet and Hajcak, 2008). Prior research has generally supported the view that ERN magnitude increases throughout adolescence and into early adulthood (for a review, see Tamnes et al., 2013). However, the neuroanatomical basis of such age-related changes in error monitoring, during the time range of the ERN, remains ambiguous. Specifically, it is unclear whether the development of error-monitoring, as measured by the ERN, is associated with changes within a relatively focal and well-defined source, such as cingulate cortex, or reflects differential activation across a network of neural regions. Answering such questions has recently been made possible by advances in electroencephalogram (EEG) source localization techniques that individually model the brain and skull, and could substantially inform increasingly complex models of error-monitoring and related processes (e.g. Shenhav et al., 2013; Weinberg et al., 2016). However, advanced source localization methods have not yet been applied to the study of error-monitoring system development.

Functional magnetic imaging (fMRI) studies have demonstrated that error processing is associated with widespread activation across a broad network of neural regions (Taylor et al., 2007). Namely, the dorsal-anterior and posterior cingulate cortex (dACC and PCC, respectively), insula, operculum, ventral and lateral prefrontal cortex, and lateral parietal cortex have all been linked to error processing in prior fMRI investigations (for a review, see Taylor et al., 2007). The dACC in particular, has been the focus of extensive research into error processing, demonstrating sensitivity to errors in both fMRI (Carter et al., 1998; Holroyd et al., 2004; Kerns et al., 2004) and single-unit recording (Ito et al., 2003; Amiez et al., 2005) investigations. Consistent with this notion, the majority of source localization studies in both children and adults have reported focal activation within the dACC (for a review, see Agam et al., 2011). However, as noted by Agam and colleagues (2011), a careful reading of the literature reveals that although many studies describe peak ERN source activity as occurring within the dACC, approximately half of the foci of these studies lay posterior to the ACC-PCC border, and a more appropriate label for these ERN sources would be "PCC". Critically, a recent report that employed MRI-constrained source-localization of the ERN, along with a distributed-source solution, identified maximal ERN-source activity within the posterior cingulate cortex (PCC), as opposed to the dACC (Agam et al., 2011). Additionally, given that several other neural regions are known to be activated

by errors (Taylor et al., 2007), it is possible that the methods that have typically been employed previously for source localization (dipole modeling with standard head models) have obscured important nuances in understanding networks involved in error monitoring.

While the ERN magnitude is believed to increase throughout adolescence and into early adulthood (Tamnes et al., 2013), prior source localization investigations of ERN development have reported a primary source within dACC that does not change as a function of age (Mathewson et al., 2005; Ladouceur et al., 2007; Santesso and Segalowitz, 2008). Thus, the same region of cingulate cortex may generate the ERN throughout adolescence and adulthood, with changes in amplitude resulting only from changes in the efficiency of this neural region. However, it is well established that widespread areas of the brain, particularly regions underlying higher cognitive functions, undergo substantial reorganization over the course of adolescence and into adulthood (Sowell et al., 1999b; Gogtay et al., 2004; Tamnes et al., 2010). Additionally, analyses of executive functioning development have demonstrated dramatic changes in network dynamics with increasing age (Fair et al., 2007, 2009). Therefore, it is possible that age-related changes in the magnitude of the scalp-recorded ERN are not driven by changes within a relatively focal and well-defined source, such as the cingulate cortex, but instead reflects differential activation across a network of neural regions. It is possible that previous investigations missed such effects, given the use of a "dipole fitting" procedure, in which the number and possible location of sources are strongly influenced by the decisions of the experimenter (for details, see Michel et al., 2004). Additionally, none of the previous developmental investigations employed realistic modeling of the brain and skull, a factor that can substantially influence source localization accuracy (Vorwerk et al., 2014; Cho et al., 2015), especially within a developmental context (Reynolds and Richards, 2009; Richards and Xie, 2015).

Development of the error-monitoring system during adolescence and early adulthood is of particular interest, given that this period is marked by an increased risk for various forms of psychopathology, including anxiety disorders, depression, psychopathy, impulse-control disorders and schizophrenia (Pine et al., 1998; Kessler et al., 2007; Merikangas et al., 2010). Critically, several forms of psychopathology that emerge in adolescence have been linked to either increases or decreases in the ERN (Gehring et al., 2000; Hall et al., 2007; Olvet and Hajcak, 2008; McDermott et al., 2009). Further, competing models exist for explaining the link between the ERN and specific forms of psychopathology, such as anxiety (Moser et al., 2013; Weinberg et al., 2016). An improved estimation of the neural source(s) generating the scalp-recorded ERN would not only help to inform more general models of error monitoring and the ERN, but also shed light on the relation between the ERN and specific forms of psychopathology. Moreover, a model of typical error-monitoring system development during adolescence and adulthood would provide a valuable reference for future studies investigating the development of psychopathology related to this system.

The current study employed MRI-constrained source localization of the ERN in order to relate variation in age from early adolescence through early adulthood to variation in functioning of the error-monitoring system. Consistent with either the prevailing view (Ullsperger et al., 2014), or recent research (Agam et al., 2011), we hypothesized that changes in the ERN would be primarily explained by a source within either the anterior or

posterior cingulate, respectively. However, given the dramatic cortical reorganization that is reflected in adolescence and early adulthood, an alternative possibility is that changes in the ERN arise from changes in distributed source activity outside of cingulate cortex.

Method

Participants

Forty-three participants ranging in age from 9.89–35.09 years (M age = 18.65, SD = 6.18, 23 females) completed the study. The participants consisted of 17 Caucasians, 13 African-Americans, 12 Asians, and one Hispanic; a one-way ANOVA model indicated no significant differences in age across the ethnic categories, $F(3,39) = 1.80$, $p = .163$. Of note, the primary analyses of this study treated age as a continuous variable. Nevertheless, where appropriate, participants were divided into four roughly equal groups (quartile split based on age) for display purposes and exploratory analyses. The four age groups were as follows: group one ($n = 10$) had an age range of 9.89–13.63 years (M age = 11.79, 6 females); group two ($n = 11$) had an age range of 14.18–15.96 years (M age = 15.02, 7 females); group three ($n = 11$) had an age range of 16.92–22.80 years (M age = 20.35, 5 females); group four ($n = 11$) had an age range of 22.95–35.09 years (M age = 26.81, 5 females).

Participants were healthy volunteers recruited from the local DC-metropolitan area and received monetary compensation for their participation. Inclusion criteria for participants included an IQ > 70 and normal physical health. The minimum IQ for participants included in the current sample was 91 ($M = 113.77$, SD = 11.34); critically, IQ did not correlate with age ($p = .285$). Additionally, participants were free of psychopathology as determined by a structured interview; the Schedule School-Age (K-SADS- PL; Kaufman et al., 1997) was used for participants 17 and younger and the Structured Clinical Interview for DSM-IV- TR Axis 1Disorders (SCID; First, Spitzer, Gibbon and Williams, 2002) for participants 18 and older. All participants over the age of 18 provided written informed consent; for participants under the age of 18, parents signed consent and youth signed assent. All procedures were approved by the Institutional Review Boards of the University of Maryland (UMD) and the National Institute of Mental Health (NIMH). Data from an additional 3 participants were collected, but not used, as the result of artifact-laden EEG (n = 1), an error during EEG recording (n = 1), or low behavioral accuracy (accuracy < 70%; n = 1).

Procedure

Participants performed a modified flanker task (Eriksen and Eriksen, 1974) at UMD while EEG data were collected; fiducial anatomical and electrode landmarks were digitized for each participant. Additionally, structural MRIs were collected for all participants at NIMH for the purpose of creating subject-specific head models for current source reconstruction. Participants also performed the flanker task while at NIMH and functional data were collected. Results of the functional study will be reported elsewhere. The order of visits to NIMH and UMD was counterbalanced across participants and the mean number of days between visits was 44 days (SD = 47 days). Reported ages reflect the age at the time of EEG acquisition.

Experimental Task, Apparatus and Stimuli

Participants completed a modified flanker task (Eriksen and Eriksen, 1974), presented using E-Prime software (Psychology Software Tools, Inc., Sharpsburg, PA). Each trial consisted of an arrow being presented in the center of the screen, flanked on either side by two arrows that were either facing in the same (congruent) direction as the central arrow, or in the opposite (incongruent) direction as the central arrow. Congruent and incongruent trials were presented randomly, with incongruent trial being presented with a 50% probability. Participants were instructed to indicate the direction of the central arrow via button press and ignore the flanking stimuli, regardless of their congruency. Participants indicated the direction of the central arrow by pressing either one of two buttons, located on an E-Prime button box, using the thumb of their left and right hands; leftward-facing arrows required a response from the left hand and rightward-facing arrows required a response from the right hand. Each trial began with the presentation of a fixation cross, which remained on screen for a variable interval of 300–600 ms. The flanker stimulus was then presented for 200 ms, followed by a blank screen for 1860 ms; participants were allotted a 1500 ms window in which to provide their response. Each arrow stimulus array subtended 8.26 by 1.77 degrees visual angle and were presented on a 34 cm by 27.5 cm LCD monitor with the resolution set at 800 x 600. The fixation cross subtended .88 by .88 degrees. The fixation cross was dark grey in color and the arrow stimuli were uniformly white; both were presented on a solid black background.

Prior to completing the experimental task, participants were explained all instructions and presented with 16 practice trials, followed by feedback. If participants performed at or below 75% accuracy they received a message to "be more accurate". If performance was at or above 90% they received a message to "Respond faster". If performance was between 75% and 90% they received a message reading "Good job". These messages were also presented following each block in the experimental task. This feedback procedure helped maintain accuracy at a level that would ensure an adequate number of errors occurred, consistent with the recommendations by Gehring and colleagues (2012). Post-hoc analyses found that accuracy rates were indeed lower on the blocks following feedback instructing participants to "respond faster" (M = 87.17%, SE = 7.07%), compared to blocks following feedback indicating that participants did a "good job" (M = 89.01%, SE = 7.31%), $t(1,40)$ = 2.70, p = .008. Critically, changes in accuracy, as a function of prior feedback, did not correlate with age (p = .159). Similarly, the number of times that participants received each type of feedback did not correlate with age (all p > .19). Following practice, participants completed 10 blocks of 32 trials each (320 trial total). Each block was followed by a short break.

EEG Acquisition and Preprocessing

EEG was acquired using a 128-channel HydroCel Geodesic Sensor Net and EGI software (Electrical Geodesic, Inc., Eugene, OR); EEG analysis was performed using the EEGLAB toolbox (Delorme and Makeig, 2004) and custom MATLAB scripts (The MathWorks, Natick, MA). Given that EEG data were acquired using a high input-impedance system, electrode impedances were maintained below 50 kΩ; data were sampled at 250 Hz, and referenced online to the vertex. Following acquisition, systematic marker offsets were measured and corrected for the EGI system (constant 36 ms offset) and E-Prime computer

(constant 15 ms offset). PREP pipeline tools (Bigdely-Shamlo et al., 2015) were used to filter out 60 Hz noise, as well as identify and remove bad channels. Data were then high-pass filtered at .3 Hz. In order to identify and remove artifactual activity from the data, ICA decomposition was run on an identical data set with the addition of a 1 Hz high-pass filter. This 1 Hz filtered data set was first epoched into arbitrary 1000 ms epochs; prior to running ICA, noisy epochs were detected and removed if amplitude was +/− 1000 uV or if power within the 20–40hz band (after Fourier analysis) was greater than 30dB. If a channel led to more than 20% of the data being rejected, this channel was instead rejected. ICA was then run on the 1 Hz high-pass filtered dataset and the ICA weights were then copied back to the original (continuous) .3 Hz high-pass filtered dataset; all subsequent processing was performed on the .3 Hz high-pass filtered dataset. Artifactual ICA components were first detected in an automated procedure using the ADJUST toolbox (Mognon et al., 2011), followed by manual inspection of the ICA components. All ICA components identified as reflecting artifacts were subtracted from the data. For ERP analyses, the data were low-pass filtered at 30hz and then epoched to the response markers from -500 to 1000 ms. All response-locked epochs were baseline corrected using the 200 ms period preceding response onset; see supplementary material for a set of control analyses demonstrating that the choice of baseline period does not qualitatively change the results. A final rejection of +/− 100 uV was used to identify and remove bad epochs in the data that might have been missed by other methods. If greater than 20% of the data were rejected, the channel was rejected instead. All missing channels were now interpolated using a spherical spline interpolation. On average, 8.96% of channels were rejected (SD = 3.78%). Following interpolation, data were referenced to the average of all electrodes. All participants included in the ERP and current source analyses had a minimum of 10 artifact-free incongruent-error trials ($M =$ 29.05, SD = 11.52), which has been shown to elicit a reliable measurement of the ERN in both children and adults (Pontifex et al., 2010; Steele et al., 2016). Further, the number of artifact-free error trials did not correlate with age (r = .216, $p =$ .164). For additional ERP analyses that included the number of correct and error trials as covariates, see the supplementary material; inclusion of trial counts led to no qualitatively different results for the effects of interest.

Fiducial Landmark Digitization

Before beginning the experimental task, three-dimensional coordinates of 14 anatomical and electrode fiducial landmarks were digitized using the Polhemus Fastrak system (Polhemus Inc., Colchster, VT). Seven anatomical fiducials that are commonly used for the 10–10 system were digitized on each participant; these locations were the naision (Nz), the inion (Iz), the left mastoid (LMA), the right mastoid (RMA), the left pre-auricular (LPA), the right pre-auricular (RPA), and the vertex (Vz). Additionally, seven electrodes of the Hydrocel Geodesic Sensor Net 128 (HGSN128) that are located near the anatomical fiducials were digitized; the electrode numbers and their approximate corresponding anatomical landmarks were 17-Nz, 75-Oz, 57-LMA, 100-RMA, 44-LPA, 115-RPA, 129-Vz (see Richards et al., 2015). The following head measurements were also taken for each participant: front and rear semi-circumferences (LMA to RMA), top circumferences (Nz to Iz, and LMA to RMA), and lateral diameters (Nz to Iz, and LMA to RMA).

MRI Acquisition

Two structural images were acquired for each participant on a 3-Tesla MR750 GE scanner with a 32-channel head coil. For each participant, a high-resolution T1-weighted magnetization-prepared rapid acquisition gradient-echo sequence (MPRAGE; sagittal acquisition; TI/TE= 425/min; flip angle = 7°; FOV = 25.6; Matrix 256x256; Slice thickness = 1mm; bandwidth = 25HTz) and a T2-weighted fast relaxation fast spin-echo sequence was acquired (FRFSE-XL; sagittal acquisition; TR/TE 15000/80 ms; FOV = 25.6; Matrix 256x256; Slice thickness = 1mm; bandwidth = 31.25HTz) was acquired. Critically, both the T1 and T2 images were acquired with an FOV that allowed for imaging the neck of the participant. As a result, regions of the neck could also be incorporated into the head model used for source localization (see below).

Behavioral Analyses

All trials in which participants did not respond, or responded within 150 ms of stimulus presentation, were removed from the analyses. Overall accuracy was calculated and one participant with accuracy below 70% was removed from subsequent analyses. To test whether the standard flanker task congruency effect for accuracy (percentage correct) was present, and whether this effect varied with age, a general linear model (GLM) was conducted, with accuracy (percentage correct) as the DV, congruency as a within-subjects factor, and age as a continuous between-subjects factor. Similarly, to test whether the standard flanker task congruency effect for correct trial response time (RT) was present, and whether this effect varied with age, a general linear model (GLM) was conducted, with RT as the DV, congruency as a within-subjects factor, and age as a continuous between-subjects factor.

In order to investigate whether individuals adapted their behavior following errors, post-error accuracy (PEA) and post-error slowing (PES) were calculated for all participants. PEA was quantified as the difference between the mean accuracy for trials immediately following incongruent-error trials and the mean accuracy for trials immediately following incongruent-correct trials. PES was quantified as the difference between the mean RT for correct trials immediately following incongruent-error trials and the mean RT for correct trials immediately following incongruent-correct trials. Tests for Pearson product-moment correlations between either PES or PEA and age were conducted. Additionally, tests for Pearson product-moment correlations between either PES or PEA and estimated source activity within each of the regions of interest (ROIs) for which source localization was analyzed were conducted; a false-discovery rate correction for multiple comparisons was applied to this family of 14 correlation tests using the method proposed by Benjamini and Hochberg (1995). To determine whether any possible relations between the source activity and post-error behavior were dependent on age, a series of follow-up partial correlation tests were conducted while controlling for age. Finally, we also tested whether the delta-ERN correlated with PEA, as well as performed an exploratory analysis on the within-subject relations between the ERN and post-error accuracy (see supplementary material).

ERP Analyses

The ERN and correct-related negativity (CRN) were separately quantified for each individual by first identifying the peak negativity occurring between -100 and 100 ms (relative to response) at a cluster of frontocentral electrodes close to the FCz location (12, 5, 6/FCz, 13/FC1, 112/FC2, 7, 106). In order to explore possible topography differences, the mean amplitude during a 40 ms window (centered on the individually defined peak) was then separately calculated for incongruent correct and incongruent error of commission trials at four midline EGI electrode locations 11/Fz, 6/FCz, 5/CPz and 62/POz that approximately correspond to FZ, FCZ, CPZ and Pz, respectively. The ERN/CRN was analyzed using a GLM, with mean amplitude as the DV, accuracy (ERN, CRN) and electrode location as within-subjects factors, and age as a continuous between-subjects factor. Where appropriate, degrees of freedom were adjusted using the Hyund-Feldt correction for violations of sphericity.

MRI Segmentation and Current Source Reconstruction

Localizing the sources of scalp-recorded ERP data required several steps, which are described in detail below as well as in previous work (Richards, 2013; Henderson et al., 2014). Briefly, our processing pipeline included the following: registering electrode locations within MRI-space, segmentation of MRI volumes, the construction of a source and head model, calculation of the inverse solution in order to determine the current density distribution, the construction of ROIs in which to analyze current density, and the statistical analysis of current density activity within predefined ROIs. The use of individualized head and source models for each participant, based on MRI segmentation, has been shown to greatly improve source localization accuracy (Vorwerk et al., 2014; Cho et al., 2015). This is particularly important within a developmental context (Reynolds and Richards, 2009; Richards and Xie, 2015), given the changes that occur in neuroanatomy throughout development (Sowell et al., 1999a, 1999b; Gogtay et al., 2004; Blakemore and Choudhury, 2006). It should also be noted that a "distributed source model" approach to source localization, as opposed to a "dipole fitting" approach, is not influenced by a priori decisions about the number or location of possible sources generating the scalp-recorded ERP activity (Michel et al., 2004). This is particularly important within a developmental context, as the neural regions contributing to a given ERP effect likely change as the result of changes in neural network architecture over the course of development (Fair et al., 2007, 2009).

Electrode registration—In order to identify each participant's electrode locations within MRI-space, the seven anatomical fiducials (Nz, Oz, LMA, RMA, LPA, RPA, Vz) were manually identified on each participant's MRI using MRIcroGL (Rorden, 2012). Additionally, the anterior commissure (AC) and posterior commissure (PC) were identified. Next, the digitized anatomical fiducials were registered to the MRI-identified fiducials using "coherent point drift" registration (Myronenko et al., 2006; Myronenko and Song, 2010). The registration matrix that resulted from registering the digitized anatomical fiducials was then used to transform the digitized electrode fiducials within MRI-space. In order to identify the locations of the remaining electrode locations within MRI-space, average electrode locations from age-appropriate average MRI templates (Richards and Xie, 2015; Richards et al., 2016) were used. The seven electrode fiducials that were now in MRI-space

were registered to the corresponding electrode coordinates in the average electrode placement template using CPD. This registration matrix was then used to transform the remaining electrodes from the average electrode location template into MRI-space for the participant. The electrode locations were then fit to the scalp by identifying the point of the scalp nearest to the transformed electrode locations and these locations were referenced to the individualized AC-coordinate system using the previously identified AC/PC locations. For more details on the electrode localization procedure see Richards and colleagues (2015).

MRI segmentation—Segmentation of the MRI volumes was performed through a combination of automated and manual procedures. Brain extraction was performed first, using BET; the BETSURF tool was used to identify and segment the head and brain surfaces within the T1 and T2 volumes (Jenkinson et al., 2012). Next, the FAST tool was used to identify the probability of each voxel containing grey matter, white matter, CSF, or other media (Jenkinson et al., 2012). Using MRIcroGL, the eyes, throat and nasal cavity were manually identified (Rorden, 2012).

Source model, head model and lead field matrix—Construction of the source model, head model, and lead field matrix were performed with the Fieldtrip software library (Oostenveld et al., 2011); all functions beginning with "ft_" in this manuscript reflect Fieldtrip functions. A volumetric source model grid with a 3 mm resolution was created within the participant's MRI-space from the segmented grey matter and eyes using the ft_prepare_sourcemodel function. Next, a volume conduction model (head model) that describes how electrical current flows through the head was constructed using the finite element method (FEM) implemented in Fieldtrip. In order to create the head model, a hexahedral mesh was created within the participant's MRI-space, such that each hexahedron was assigned membership to one of the nine possible segmented media types (grey matter, white matter, CSF, dura, skull, scalp, eyes, throat/nasal cavity, or muscle). Following creation of this full-head mesh, a "SIMBIO" FEM head model that associates conductivity values with each tissue type was created using ft_prepare_headmodel. Finally, the lead field matrix (forward solution) was constructed by combing the source model, head model, and electrode locations using ft_prepare_leadfield.

Inverse solution—The inverse solution was calculated using ft_sourceanalysis with the exact low-resolution electromagnetic tomography (eLORETA) method (Pascual-Marqui, 2007; Pascual-Marqui et al., 2011) as the constraint on the inverse solution. This yielded a dipole moment vector at each source volume grid location, which was further converted to a power value representing the current density at that location for a given time point. The inverse solution was conducted for each sample within the 40 ms window for which the scalp-recorded EEG was analyzed and the resulting current density reconstruction (CDR) values were then averaged over each time point to identify the average source activity during this 40 ms window. Additionally, in order to plot the CDR activity surrounding the ERN/CRN peak, and identify whether the source activity peaked at a similar time point as the scalp-recorded EEG, CDR values were calculated for an additional 15 samples (60 ms) before and after the ERN/CRN time window. Because the CDR technique yields current activity within the source model, as opposed to voltage, it is critical to rebaseline ERP data

prior to conducting CDR in order to ensure that the CDR solution represents a scalp-recorded relative negativity. To this end, the positivity immediately preceding the ERN or CRN peak for each individual was identified and the amplitude obtained from 3-samples (12 ms) centered on this peak were subtracted from each participant's ERP prior to calculating the inverse solution; see the supplementary material for an analysis demonstrating that this positivity did not significantly differ as a function of any conditions of interest. Three samples (12 ms) were used in the re-baseline procedure as a compromise between the increased reliability of using more samples, while also not overlapping with the component of interest by using too wide of a window. The inverse solution was separately calculated for correct and error trials, and not a difference wave, allowing separate localization of the ERN and CRN sources. Once the CDR values for the ERN and CRN were identified, it was then possible to subtract these sources for visualization purposes or for analysis within a given ROI.

ROI construction and statistical analysis—Based on prior research investigating error-related neural activity, we employed an ROI approach for analysis of the CDR data. ROIs were defined for each individual participant's brain using a combination of atlases in subject-specific MRI-space. First, three atlases, the LONI Probabilistic Brain Atlas (LPBA; Shattuck et al., 2008), the Hammers atlas (Hammers et al., 2003; Heckemann et al., 2006) and a lobar atlas were constructed on individual participants using the method described in Fillmore and colleagues (2015). Additionally, the Harvard-Oxford and Brodmann atlases, available from the FSL library (Jenkinson et al., 2012), were transformed from the MNI152 atlas to an age-appropriate atlas, followed by further transformation into subject-specific MRI-space. Based on the review of error-monitoring by Taylor and colleagues (2007), a combination of these five atlases was used to identify a total of 23 ROIs on the subject-specific MRI. Further, an a priori decision was made to average over activity within bilateral ROIs in order to reduce the number of comparisons being made and control the false-positive rate. This process yielded 14 ROIs, which reflects the optimal compromise between a focused analysis of error-related brain activity on the one hand, and a minimization of a priori judgments about the possible source(s) of the ERN. The 14 ROIs for which statistical analyses were conducted are as follows: frontal pole, bi-lateral insula, bilateral inferior frontal gyrus, orbital frontal gyrus, ventral anterior cingulate, dorsal anterior cingulate, posterior cingulate, bi-lateral frontal eye fields, bi-lateral dorsolateral prefrontal gyrus, bi-lateral precentral and postcentral gyrus, bi-lateral superior parietal lobe, bi-lateral supramarginal gyrus, bi-lateral angular gyrus, bilateral intraprarietal sulcus; these ROIs are listed in table 1 along with the corresponding labels from the five atlases. Following the initial a priori analyses of these 14 ROIs, subsequent exploratory analyses were performed for ROIs yielding significant changes in estimated source activity as a function of age in order to explore possible laterality effects.

Following calculation of CDR values across the entire source volume, power values at each dipole within a given ROI were summed and then divided by the total volume of that ROI (bilateral ROIs were subsequently averaged together). This approach yielded a separate current per mm^3 value for each of the 14 ROIs, for correct (CRN) and error (ERN) responses. ROI-based CDR values were then analyzed using a GLM, with current per mm^3

as the DV, accuracy (ERN, CRN) and ROI as within-subjects factors, and age as a continuous between-subjects factor. Where appropriate, degrees of freedom were adjusted using the Hyund-Feldt correction for violations of sphericity. Given that a three-way interaction between accuracy, ROI and age was identified (see results section) follow-up correlations between error-correct CDR difference score activity in each ROI and age were tested; a false-discovery rate correction for multiple comparisons was applied to this family of 14 correlation tests.

Results

Behavior

Mean accuracy was 88.56% (SD = 3.89%). Analysis of the accuracy data revealed a main effect of congruency [$F(1, 41) = 19.48$, $p < .001$)], such that congruent trials ($M = 97.40\%$, SD = 0.40%) were more accurate than incongruent trials ($M = 79.72\%$, SD = 1.03%). Neither a main effect of age ($p = .311$), or an interaction between age and congruency ($p = .428$) were identified for accuracy. Analysis of RT data for correct trials revealed a main effect of congruency [$F(1, 41) = 20.71$, $p < .001$)], such that participants responded faster on congruent trials ($M = 360.13$ ms, SD = 6.26 ms) compared to incongruent trials ($M = 428.43$ ms, SD = 8.24 ms). Additionally, a main effect of age was identified [$F(1, 41) = 6.09$, $p = .018$)], such that age was negatively correlated with overall correct trial RT ($r = −.360$, $p = .018$). This negative relation between RT and age suggests that increasing age is associated with improved task performance, possibly due to enhanced motivation. No interaction between age and congruency was identified for RT ($p = .372$). Tests for correlations between age and post-error behavior revealed no relationship for either PEA ($r = −.044$, $p = .782$) or PES ($r = .212$, $p = .172$). On average, no significant PES [$t(1, 42) = 0.57$, $p = .571$)], nor PEA [$t(1, 42) = .36$, $p = .718$)], was identified. Nonetheless, substantial variation for both PES (SD = 17.28 ms) and PEA (SD = 7.04%) was present, and prior work has demonstrated that brain-behavior relations can still exist in the absence of significant contextual effects at the group level (Buzzell et al., 2016). In the section below, entitled "brain-behavior relations", we report significant correlations between neural activity and PEA.

ERP Results

Analysis of the ERP data during the time range of the ERN revealed an interaction between electrode and accuracy [$F(3, 123) = 15.89$, $p < .001$)]. Consistent with prior literature, the interaction between electrode and accuracy was such that, regardless of age, participants demonstrated a maximal difference between error and correct incongruent responses over frontocentral (11/Fz and 6/FCz) electrode locations. However, the accuracy by electrode interaction was qualified by a three-way interaction between electrode, accuracy and age [$F(3, 123) = 7.64$, $p = .001$)]. Post-hoc correlations between delta-ERN (error minus correct) activity and age at each of the four electrode locations revealed that the error minus correct effect only correlated with age at the centroparietal electrodes, 5/CPz ($r = −.433$, $p = .004$) and 62/POz ($r = −.512$, $p < .001$). Thus, all participants demonstrated a classic frontocentral ERN effect, but the topography of the ERN effect differed with age; increasing age was associated with more posterior electrodes also demonstrating this effect. No other significant main effects or interactions were identified for the GLM analysis of the ERP data. Figures 1

and 2 depict both grand average and age-related changes within the ERP activity; although statistical analysis of age related-changes treated age as a continuous variable, a quartile-split was used to display changes in ERP activity as a function of age.

Source Localization Results

Analysis of the CDR data revealed an interaction between accuracy (ERN, CRN) and ROI [$F(13, 533) = 2.65$, $p = .039$)]. The nature of this interaction was such that, regardless of age, a maximal difference between error and correct trial activity was identified within the PCC. Figure 3 depicts the grand-average source localization results, demonstrating maximal activation within PCC. Additionally, figure 3c displays the time course of source activity within two exemplar ROIs (PCC and dACC) in which ERN/CRN activity peaked within source space at the same time as at the scalp-recorded ERP components. In contrast, the time course of source activity within the angular gyrus demonstrates no clear peak within source space and a minimal difference between the ERN and CRN.

The interaction between accuracy and ROI for the CDR data was qualified by a three-way interaction between accuracy, ROI and age [$F(13, 533) = 2.71$, $p = .036$)]. Post-hoc correlations between error minus correct CDR activity in each ROI and age revealed a significant correlation for activity within the insula ($r = .433$, $p = .004$), orbitofrontal gyrus ($r = .417$, $p = .005$), and inferior frontal gyrus ($r = .421$, $p = .005$); see table 2 for a list of all correlation coefficients. In order to explore possible laterality effects, post-hoc analyses were also performed for the two bilateral regions that revealed significant relations between source activity and age: the insula and the inferior frontal gyrus. However, similar correlations were found between each homologous ROI and age: left insula ($r = .459$, $p = .002$), right insula ($r = .312$, $p = .042$), left inferior frontal gyrus ($r = .382$, $p = .012$), and right inferior frontal gyrus ($r = .387$, $p = .01$). Notably, there were no age effects for activity within the dACC or posterior cingulate. No other significant main effects or interactions were identified for the GLM analysis of the CDR data. Figure 4 depicts age-related changes within source activity; although the analysis of age related-changes treated age as a continuous variable, a quartile-split was used to display changes in source activity as a function of age. Whereas clear age-related increases in ventral-frontal brain regions can be seen in figure 4, apparent differences between the youngest age group and the other three age groups is also observed. A series of exploratory independent-samples t-tests were performed to investigate possible differences in ROI source activity between the youngest age group and each of the other age groups for all 14 ROIs. However, the only significant differences identified (not corrected for multiple comparisons) were for comparisons between the youngest and oldest age groups within the insula ($p = .049$), inferior frontal gyrus ($p = .016$) and the precentral/postcentral gyrus ($p = .045$). Thus, many of the apparent differences between the youngest age group and the other three age groups are not statistically significant. Instead, age-related changes within the sources of the ERN/CRN are best described by relative stability in a number of frontal and parietal brain regions, accompanied by robust linear increases in ventral-frontal activity across the age range studied.

Brain-behavior Relations

Testing for correlations between error minus correct activity for each ROI and PEA revealed significant correlations for activity within several regions, including dACC ($r = .364$, $p = .016$), PCC ($r = .353$, $p = .020$), superior parietal cortex ($r = .417$, $p = .005$), supramarginal gyrus ($r = .469$, $p = .002$), angular gyrus ($r = .450$, $p = .002$), and intraparietal sulcus ($r = .505$, $p < .001$); see table 2 for a list of all correlation coefficients and figure 5 for scatter plots of all significant correlations. Critically, all of these correlations remained significant when an additional set of correlations were tested in which age was also controlled for; the DLPFC also reached significance when age was controlled for (see table 2). These results suggest that activity within a frontoparietal network, including cingulate and parietal cortex, is predictive of improved task performance following errors, regardless of age. Correlations between CDR activity and PES were also tested but no significant correlations were identified (see table 2). Relations between the delta-ERN and PEA were also found to be in the expected direction, but were not significant at either electrode 11/FZ ($r = -.241$, $p = .120$) or 6/FCz ($r = -.175$, $p = .261$). However, we also performed an additional analysis in which the ERN was binned based on whether the subsequent trial was correct or not (i.e. a within-subjects analysis of the relation between the ERN and PEA) and found that the ERN was significantly more negative for error trials that were followed by a correct response, compared to error trials that were followed by another error, ($p = .044$; see supplementary material).

Discussion

The current study investigated age-related variation of the error-monitoring system throughout adolescence and adulthood using an ERP approach and leveraging MRI-constrained source localization of the ERN. Consistent with the prevailing view that dACC activity drives the ERN (Ullsperger et al., 2014), the ERN was localized, in part, to the dACC. However, the maximal generator of the ERN was localized to PCC, and error-related activity was also observed within several other frontal and parietal regions. Critically, these results are consistent with recent research (Agam et al., 2011) and the prior reports of error-related neural activity outside of the cingulate cortex (Taylor et al., 2007). The link between error-monitoring and cognitive control (Botvinick et al., 2004) was also observed, with activity within a fronto-parietal network positively correlating with improved performance following errors. Critically, the relation between the activity of this fronto-parietal network and PEA was independent of age. Additionally, activation throughout the cingulate and parietal cortex, regardless of post-error behavior, did not vary as a function of age. Age was only associated with linear increases in insula, OFC and IFG activity. Collectively, these results demonstrate that the core error-monitoring system is relatively stable throughout adolescence and early adulthood, whereas linear changes in regions of the ventral-frontal cortex related to affective/salience processing (Seeley et al., 2007) or inhibition (Aron et al., 2004) continue to occur during this period. The bifurcated developmental pattern observed here can serve as a template for studies investigating the relation between error-monitoring dysfunction and the onset of psychopathology in adolescence or adulthood.

Analysis of the ERP data alone revealed several interesting findings. Across the age range studied, all individuals demonstrated a frontocentral difference between the ERN and CRN (delta-ERN), consistent with other research (Gehring et al., 2012). However, age-related increases in the delta-ERN were only significant at centroparietal electrode locations. The finding that age was exclusively correlated with the delta-ERN at centroparietal locations is consistent with research by Davies and colleagues (2004), which demonstrated that the ERN was largest for adults at central electrode locations, whereas children exhibited a more frontal ERN. The current report extends prior work by also showing that the delta-ERN directly correlates with age, and that such a relation is only present at more posterior electrode locations. Given, that a change in topography necessarily implies a change in neural source activity, the ERP data alone demonstrate that the neural sources of the ERN change with age.

Source localization of the ERN revealed activation within a network of frontal and parietal regions, with maximal activation residing in PCC. Although previous research has generally suggested that the ERN reflects a singular source within dACC, most prior research has used dipole fitting procedures that do not utilize realistic head models (see review in Agam et al., 2011). Additionally, fMRI studies commonly identify error-related activity in a number of regions outside the dACC (Taylor et al., 2007) and a recent MEG source analysis study also localized error/loss feedback to PCC (Donamayor et al., 2011). An independent source imaging study that recorded EEG, MEG and fMRI, localized the primary source of the ERN to the PCC and found that the ERN was correlated with both dACC and PCC fMRI activity (Agam et al., 2011). Additionally, Agam and colleagues (2011) demonstrated that current source estimates within the dACC peaked significantly *later* than source estimates within the PCC, and that dACC and PCC fMRI activity were functionally linked. Taken together with the observation that ERN magnitude is predicted by the myelination of white matter within the posterior cingulum bundle (Westlye et al., 2009), these findings suggest that the ERN is generated within the PCC first and then relayed to the dACC. The current study provides additional evidence for a maximal source of the ERN within the PCC, in conjunction with error-related source activity within the dACC and an extended network of neural locations. Activation within a broad network of cortical regions during the ERN time range is consistent with studies that have linked cortical regions outside of the dACC to the ERN. For example, Liu and colleagues (2014) demonstrated that grey matter within the insula and OFC were correlated with ERN magnitude, whereas Gehring and Knight (2000) have shown that damage to lateral prefrontal cortices leads to reduction in ERN magnitude. These results are not inconsistent with the prevailing view that the dACC plays a primary role in error-monitoring and the generation of the ERN (Ullsperger et al., 2014), rather, these data expand this view by broadening the neural network that is thought to give rise to error-monitoring and generation of the scalp-recorded ERN.

Error monitoring is typically viewed as a necessary first step before cognitive control can be instantiated to prevent future errors (Shenhav et al., 2013). In line with prior research (King et al., 2010), the present study found that activity within a network of regions, including dACC, PCC and several parietal regions, correlated with improved performance on post-error trials. That is, the classic relation between monitoring and control was observed (Botvinick et al., 2004). The observed link between neural activity within the cingulate

cortex and control on the subsequent trial is a well-established phenomenon (Carter et al., 1998; King et al., 2010; Danielmeier et al., 2011), and provides corroborating evidence for the reliability of the source-localization results. Interestingly, the monitoring-control relation was independent of participant age. Additionally, several of the most highly active ERN sources, including activity within the PCC and the rest of the cingulate, did not vary as a function of age. Instead, the only cortical regions that exhibited age-related changes in error-evoked activity were the insula, IFG and OFC. Collectively, these results suggest that the core error-monitoring system, and its relation to cognitive control, does not undergo substantial change over the course of adolescence and early adulthood. Instead, a selective subset of ventral-frontal ERN sources continue to exhibit age-related changes in their error-related activity patterns during this period. The finding that the core error-monitoring system is relatively stable across adolescence and early adulthood is consistent with prior source localization studies, which demonstrate a relatively stable dACC source for the ERN across age. However, the improved accuracy of the source localization technique employed in the current study made it possible to also identify a distinct fronto-central subset of regions that exhibit changes with age.

Prior research has demonstrated that many of the frontal and parietal regions that make up the core error-monitoring system do indeed exhibit extended development throughout adolescence (Bunge and Crone, 2009; Luna et al., 2010; Somerville and Casey, 2010). However, it is important to note that much of the work of developmental neuroscience has relied on an MRI/fMRI approach (Luna et al., 2010), a neuroimaging technique with relatively limited temporal resolution. In contrast, the high temporal resolution of ERPs (Luck, 2014) provides unique insight into the dynamics of error monitoring. The neurocognitive process termed "error monitoring" is immediately preceded by error commission and often immediately followed by corrective behavior or the application of cognitive control (Van Veen and Carter, 2006). Therefore, the selective study of error monitoring, as opposed to error commission or cognitive control, is aided by the high temporal precision of the ERP technique. MRI-constrained source localization maintains the temporal resolution of ERPs while also substantially improving spatial resolution. Using such an approach, we were able to identify that, at least for the neural activity closely locked in time to "error monitoring", the core error-monitoring system displays a high level of stability across adolescence and into adulthood. Conversely, error monitoring appears to be associated with linear increases for neural activity within the insula, inferior frontal gyrus and orbitofrontal cortex during this same age range. Given the specificity of these claims, the current results remain consistent with MRI/fMRI studies indicating that frontal and parietal regions continue to exhibit more general changes related to cognitive control throughout adolescence (Bunge and Crone, 2009; Luna et al., 2010; Somerville and Casey, 2010).

The OFC and insula have well-established roles in interoceptive, affective and saliency processing. The OFC in particular has been implicated in emotional processing (Bechara et al., 2000) and specifically in linking reward (or lack thereof) to hedonic feelings (Kringelbach, 2005). Further, a recent review has suggested that the OFC may play a critical role in achieving goal-directed behavior, contingent on the motivational context (Holroyd and Yeung, 2012). In line with this notion, Hajcak and colleagues (2005) have shown that ERN magnitude is dependent on the affective or motivational significance of an error.

Similarly, Hogan and colleagues (2005) have suggested that age-related changes in the ERN may reflect differences in motivation, a notion that is further corroborated by the negative relation between RT and age in the current study. Aside from the OFC, insula activity is commonly observed in fMRI studies of error commission (Taylor et al., 2007) and is thought to directly relate to interoceptive processing (Critchley et al., 2004). The insula is a central hub within the "salience network" and plays a critical role in detecting motivationally important events that require attention (Menon and Uddin, 2010). The OFC is also part of the salience network (Seeley et al., 2007) and increasing activation of both the insula and OFC across adolescence and early adulthood is consistent with the notion that increasing age is associated with an enhanced affective/saliency response to errors, which form an integral part of motivated behavior. This interpretation is consistent with work by Hogan and colleagues (2005) that suggests that age-related changes in the ERN reflect changes in motivation.

Activation within bi-lateral IFG was also shown to linearly increase with age, however, the functional interpretation of this effect is not immediately clear. Studies have associated either right (Aron et al., 2004) or left (Swick et al., 2008) IFG activation with inhibitory control. It is therefore possible that error-related IFG activity reflects an attempt to correct the erroneous response through inhibition of motor programs. Such an interpretation is in line with prior research demonstrating that ERN magnitude is predictive of error-correction rates (Gehring et al., 1993). Although error-correction data were not collected in the current study, it has previously been shown that error-correction rates do increase with age (Hogan et al., 2005), providing indirect support for a link between IFG activity and error-correction in the current dataset. An alternative possibility is that the apparent IFG activity reflects activation within a larger cluster spanning the IFG and nearby insula. In line with this notion, a number of studies have linked interoception to activity within a neural cluster spanning the frontal operculum subdivision of the IFG and the insula (Critchley et al., 2004). If this secondary interpretation were correct, then it would be in line with the more general notion that increasing age is associated with an increased affective/saliency response to errors, possibly related to motivational changes (Hogan et al., 2005). Again, this interpretation is consistent with the finding that increasing age was associated with faster responding in the current study. Future research will be required to confirm the exact role of error-related IFG activity and its association with development.

The bifurcated pattern of error-monitoring system development observed here has several important implications for the study of developmental psychopathology, as well as models of the ERN more generally. First, longstanding debate surrounding the functional role of the ERN posit either conflict (Botvinick et al., 2001) or expectancy-based (Alexander and Brown, 2011) interpretations of the ERN on the one hand (with a focus on the cingulate cortex), or valence-based interpretations that suggest influence from more ventral neural sources on the other (Holroyd and Coles, 2002). While these views have often been difficult to integrate into a coherent model of the ERN, the present results present a natural synthesis of these theories; the current study demonstrates that the ERN is composed of both a core system centered on the cingulate cortex, as well as a more ventral set of neural sources that exhibit a dissociable developmental trajectory. In relation to psychopathology, a prominent theory of within-subject variation in the ERN suggests that variation in this component

reflects variation in sensitivity to endogenous threat (Weinberg et al., 2016). The current results present a natural extension of this theory, suggesting that variation in the ERN due threat-sensitivity may be primarily driven by the more ventral cluster of ERN activation observed here (i.e. the insula and OFC). Consistent with this notion, both the OFC and insula have been associated with interoceptive processing (Bechara et al., 2000; Critchley et al., 2004).

Although the present report extends the current understanding of how the error-monitoring system develops, a few limitations of this study should be acknowledged. First, the sample size of the current study is relatively small, considering the age range that was studied and the use of a cross-sectional design. Additionally, it is important to note that a modified flanker task was employed and researchers should exhibit caution when generalizing the current findings to other tasks. Future research could build upon the present results by employing a similar MRI-constrained source localization approach to study error-monitoring system development using an expanded sample size or within a longitudinal context, as well as in relation to psychopathology.

The current study details a neurotypical model of age-related variation in the error-monitoring system over the course of adolescence and early adulthood. Critically, the results demonstrate that healthy individuals observe a relatively strong degree of stability in the core error-monitoring system across this developmental period. Additionally, linear changes in activity of the insula, OFC and IFG are also exhibited. The observed dichotomy between a stable fronto-parietal system and a set of continually changing ventral-frontal regions provides a useful framework for conceptualizing error-monitoring system development during adolescence and early adulthood. Given that adolescence and early adulthood is a period associated with an increased risk for various psychological disorders (Pine et al., 1998; Kessler et al., 2007; Merikangas et al., 2010), which have been linked to the error-monitoring system (Gehring et al., 2000; Hall et al., 2007; Olvet and Hajcak, 2008; McDermott et al., 2009), the current results and conceptual framework provide a valuable reference for past and future clinical studies.

Supplementary Material

Refer to Web version on PubMed Central for supplementary material.

Acknowledgments

References

Agam Y, Hamalainen MS, Lee AKC, Dyckman KA, Friedman JS, Isom M, Makris N, Manoach DS. Multimodal neuroimaging dissociates hemodynamic and electrophysiological correlates of error processing. Proc Natl Acad Sci. 2011; 108:17556–17561. [PubMed: 21969565]

Alexander WH, Brown JW. Medial prefrontal cortex as an action-outcome predictor. Nat Neurosci. 2011; 14:1338–1344. [PubMed: 21926982]

Amiez C, Joseph J-P, Procyk E. Anterior cingulate error-related activity is modulated by predicted reward. Eur J Neurosci. 2005; 21:3447–3452. [PubMed: 16026482]

Aron AR, Robbins TW, Poldrack RA. Inhibition and the right inferior frontal cortex. Trends Cogn Sci. 2004; 8:170–177. [PubMed: 15050513]

Bechara A, Damasio H, Damasio AR. Emotion, decision making and the orbitofrontal cortex. Cereb Cortex. 2000; 10:295–307. [PubMed: 10731224]

Benjamini Y, Hochberg Y. Controlling the false discovery rate: a practical and powerful approach to multiple testing. J R Stat Soc Ser B Methodol. 1995:289–300.

Bigdely-Shamlo N, Mullen T, Kothe C, Su K-M, Robbins KA. The PREP pipeline: standardized preprocessing for large-scale EEG analysis. Front Neuroinformatics. 2015:9.

Blakemore S-J, Choudhury S. Development of the adolescent brain: implications for executive function and social cognition. J Child Psychol Psychiatry. 2006; 47:296–312. [PubMed: 16492261]

Botvinick MM, Braver TS, Barch DM, Carter CS, Cohen JD. Conflict monitoring and cognitive control. Psychol Rev. 2001; 108:624. [PubMed: 11488380]

Botvinick MM, Cohen JD, Carter CS. Conflict monitoring and anterior cingulate cortex: an update. Trends Cogn Sci. 2004; 8:539–546. [PubMed: 15556023]

Bunge SA, Crone EA. Neural correlates of the development of cognitive control. Neuroimaging Dev Clin Neurosci. 2009:22–37.

Buzzell GA, Roberts DM, Fedota JR, Thompson JC, Parasuraman R, McDonald CG. Uncertainty-dependent activity within the ventral striatum predicts task-related changes in response strategy. Cogn Affect Behav Neurosci. 2016; 16:219–233. [PubMed: 26453582]

Carter CS, Braver TS, Barch DM, Botvinick MM, Noll D, Cohen JD. Anterior cingulate cortex, error detection, and the online monitoring of performance. Science. 1998; 280:747–749. [PubMed: 9563953]

Cho J-H, Vorwerk J, Wolters CH, Knösche TR. Influence of the head model on EEG and MEG source connectivity analyses. NeuroImage. 2015; 110:60–77. [PubMed: 25638756]

Critchley HD, Wiens S, Rotshtein P, Öhman A, Dolan RJ. Neural systems supporting interoceptive awareness. Nat Neurosci. 2004; 7:189–195. [PubMed: 14730305]

Danielmeier C, Eichele T, Forstmann BU, Tittgemeyer M, Ullsperger M. Posterior medial frontal cortex activity predicts post-error adaptations in task-related visual and motor areas. J Neurosci. 2011; 31:1780–1789. [PubMed: 21289188]

Davies PL, Segalowitz SJ, Gavin WJ. Development of Response-Monitoring ERPs in 7- to 25-Year-Olds. Dev Neuropsychol. 2004; 25:355–376. [PubMed: 15148003]

Delorme A, Makeig S. EEGLAB: an open source toolbox for analysis of single-trial EEG dynamics including independent component analysis. J Neurosci Methods. 2004; 134:9–21. [PubMed: 15102499]

Donamayor N, Marco-Pallarés J, Heldmann M, Schoenfeld MA, Münte TF. Temporal dynamics of reward processing revealed by magnetoencephalography. Hum Brain Mapp. 2011; 32:2228–2240. [PubMed: 21305665]

Eriksen BA, Eriksen CW. Effects of noise letters upon the identification of a target letter in a nonsearch task. Percept Psychophys. 1974; 16:143–149.

Fair DA, Cohen AL, Power JD, Dosenbach NUF, Church JA, Miezin FM, Schlaggar BL, Petersen SE. Functional Brain Networks Develop from a "Local to Distributed" Organization. PLOS Comput Biol. 2009; 5:e1000381. [PubMed: 19412534]

Fair DA, Dosenbach NUF, Church JA, Cohen AL, Brahmbhatt S, Miezin FM, Barch DM, Raichle ME, Petersen SE, Schlaggar BL. Development of distinct control networks through segregation and integration. Proc Natl Acad Sci. 2007; 104:13507–13512. [PubMed: 17679691]

Falkenstein M, Hohnsbein J, Hoormann J, Blanke L, et al. Effects of errors in choice reaction tasks on the ERP under focused and divided attention. Psychophysiological Brain Res. 1990; 1:192–195.

Fillmore PT, Richards JE, Phillips-Meek MC, Cryer A, Stevens M. Stereotaxic Magnetic Resonance Imaging Brain Atlases for Infants from 3 to 12 Months. Dev Neurosci. 2015; 37:515–532. [PubMed: 26440296]

Gehring WJ, Goss B, Coles MGH, Meyer DE, Donchin E. A Neural System for Error Detection and Compensation. Psychol Sci. 1993; 4:385–390.

Gehring WJ, Himle J, Nisenson LG. Action-Monitoring Dysfunction in Obsessive-Compulsive Disorder. Psychol Sci. 2000; 11:1–6. [PubMed: 11228836]

Gehring WJ, Knight RT. Prefrontal cingulate interactions in action monitoring. Nat Neurosci. 2000; 3:516–520. [PubMed: 10769394]

Gehring WJ, Liu Y, Orr JM, Carp J. The error-related negativity (ERN/Ne). Oxf Handb Event-Relat Potential Compon. 2012:231–291.

Gogtay N, Giedd JN, Lusk L, Hayashi KM, Greenstein D, Vaituzis AC, Nugent TF, Herman DH, Clasen LS, Toga AW, Rapoport JL, Thompson PM. Dynamic mapping of human cortical development during childhood through early adulthood. Proc Natl Acad Sci U S A. 2004; 101:8174–8179. [PubMed: 15148381]

Hajcak G, Moser JS, Yeung N, Simons RF. On the ERN and the significance of errors. Psychophysiology. 2005; 42:151–160. [PubMed: 15787852]

Hall JR, Bernat EM, Patrick CJ. Externalizing Psychopathology and the Error-Related Negativity. Psychol Sci. 2007; 18:326–333. [PubMed: 17470258]

Hammers A, Allom R, Koepp MJ, Free SL, Myers R, Lemieux L, Mitchell TN, Brooks DJ, Duncan JS. Three-dimensional maximum probability atlas of the human brain, with particular reference to the temporal lobe. Hum Brain Mapp. 2003; 19:224–247. [PubMed: 12874777]

Heckemann RA, Hajnal JV, Aljabar P, Rueckert D, Hammers A. Automatic anatomical brain MRI segmentation combining label propagation and decision fusion. NeuroImage. 2006; 33:115–126. [PubMed: 16860573]

Henderson JM, Luke SG, Schmidt J, Richards JE. Co-registration of eye movements and event-related potentials in connected-text paragraph reading. Eye Mov-Relat Brain Act Percept Cogn Process. 2014:67.

Hogan AM, Vargha-Khadem F, Kirkham FJ, Baldeweg T. Maturation of action monitoring from adolescence to adulthood: an ERP study. Dev Sci. 2005; 8:525–534. [PubMed: 16246244]

Holroyd CB, Coles MGH. The neural basis of human error processing: Reinforcement learning, dopamine, and the error-related negativity. Psychol Rev. 2002; 109:679–709. [PubMed: 12374324]

Holroyd CB, Nieuwenhuis S, Yeung N, Nystrom L, Mars RB, Coles MG, Cohen JD. Dorsal anterior cingulate cortex shows fMRI response to internal and external error signals. Nat Neurosci. 2004; 7:497. [PubMed: 15097995]

Holroyd CB, Yeung N. Motivation of extended behaviors by anterior cingulate cortex. Trends Cogn Sci. 2012; 16:122–128. [PubMed: 22226543]

Ito S, Stuphorn V, Brown JW, Schall JD. Performance Monitoring by the Anterior Cingulate Cortex During Saccade Countermanding. Science. 2003; 302:120–122. [PubMed: 14526085]

Jenkinson M, Beckmann CF, Behrens TEJ, Woolrich MW, Smith SM. FSL. NeuroImage. 2012; 62:782–790. [PubMed: 21979382]

Jin J, Narayanan A, Perlman G, Luking K, DeLorenzo C, Hajcak G, Klein DN, Kotov R, Mohanty A. Orbitofrontal Cortex Activity and Connectivity Predict Future Depression Symptoms in Adolescence. Biol Psychiatry Cogn Neurosci Neuroimaging. 2017

Kerns JG, Cohen JD, MacDonald AW, Cho RY, Stenger VA, Carter CS. Anterior cingulate conflict monitoring and adjustments in control. Science. 2004; 303:1023–1026. [PubMed: 14963333]

Kessler RC, Amminger GP, Aguilar – Gaxiola S, Alonso J, Lee S, Ustun TB. Age of onset of mental disorders: A review of recent literature. Curr Opin Psychiatry. 2007; 20:359–364. [PubMed: 17551351]

King JA, Korb FM, von Cramon DY, Ullsperger M. Post-Error Behavioral Adjustments Are Facilitated by Activation and Suppression of Task-Relevant and Task-Irrelevant Information Processing. J Neurosci. 2010; 30:12759–12769. [PubMed: 20861380]

Kringelbach ML. The human orbitofrontal cortex: linking reward to hedonic experience. Nat Rev Neurosci. 2005; 6:691–702. [PubMed: 16136173]

Ladouceur CD, Dahl RE, Carter CS. Development of action monitoring through adolescence into adulthood: ERP and source localization. Dev Sci. 2007; 10:874–891. [PubMed: 17973802]

Liu Y, Hanna GL, Carrasco M, Gehring WJ, Fitzgerald KD. Altered relationship between electrophysiological response to errors and gray matter volumes in an extended network for error-processing in pediatric obsessive-compulsive disorder: ERN and VBM in Pediatric OCD. Hum Brain Mapp. 2014; 35:1143–1153. [PubMed: 23418104]

Luck, SJ. An introduction to the event-related potential technique. MIT press; 2014.

Luna B, Padmanabhan A, O'Hearn K. What has fMRI told us about the Development of Cognitive Control through Adolescence? Brain Cogn. 2010; 72:101. [PubMed: 19765880]

Maier ME, Yeung N, Steinhauser M. Error-related brain activity and adjustments of selective attention following errors. NeuroImage. 2011; 56:2339–2347. [PubMed: 21511043]

Mathewson KJ, Dywan J, Segalowitz SJ. Brain bases of error-related ERPs as influenced by age and task. Biol Psychol. 2005; 70:88–104. [PubMed: 16168253]

McDermott JM, Perez-Edgar K, Henderson HA, Chronis-Tuscano A, Pine DS, Fox NA. A history of childhood behavioral inhibition and enhanced response monitoring in adolescence are linked to clinical anxiety. Biol Psychiatry. 2009; 65:445–448. [PubMed: 19108817]

Menon V, Uddin LQ. Saliency, switching, attention and control: a network model of insula function. Brain Struct Funct. 2010; 214:655–667. [PubMed: 20512370]

Merikangas KR, He J, Burstein M, Swanson SA, Avenevoli S, Cui L, Benjet C, Georgiades K, Swendsen J. Lifetime Prevalence of Mental Disorders in US Adolescents: Results from the National Comorbidity Study-Adolescent Supplement (NCS-A). J Am Acad Child Adolesc Psychiatry. 2010; 49:980–989. [PubMed: 20855043]

Michel CM, Murray MM, Lantz G, Gonzalez S, Spinelli L, Grave de Peralta R. EEG source imaging. Clin Neurophysiol. 2004; 115:2195–2222. [PubMed: 15351361]

Mognon A, Jovicich J, Bruzzone L, Buiatti M. ADJUST: An automatic EEG artifact detector based on the joint use of spatial and temporal features. Psychophysiology. 2011; 48:229–240. [PubMed: 20636297]

Moser JS, Moran TP, Schroder HS, Donnellan MB, Yeung N. On the relationship between anxiety and error monitoring: a meta-analysis and conceptual framework. 2013

Myronenko A, Song X. Point set registration: Coherent point drift. IEEE Trans Pattern Anal Mach Intell. 2010; 32:2262–2275. [PubMed: 20975122]

Myronenko, A., Song, X., Carreira-Perpinán, MA. Advances in Neural Information Processing Systems. 2006. Non-rigid point set registration: Coherent point drift; p. 1009-1016.

Olvet DM, Hajcak G. The error-related negativity (ERN) and psychopathology: Toward an endophenotype. Clin Psychol Rev. 2008; 28:1343–1354. [PubMed: 18694617]

Oostenveld R, Fries P, Maris E, Schoffelen J-M. FieldTrip: Open Source Software for Advanced Analysis of MEG, EEG, and Invasive Electrophysiological Data. Comput Intell Neurosci. 2011; 2011:1–9. [PubMed: 21837235]

Pascual-Marqui, RD. [Accessed November 2, 2016] Discrete, 3D distributed, linear imaging methods of electric neuronal activity. Part 1: exact, zero error localization. 2007. ArXiv Prepr ArXiv07103341 Available at: http://arxiv.org/abs/0710.3341

Pascual-Marqui RD, Lehmann D, Koukkou M, Kochi K, Anderer P, Saletu B, Tanaka H, Hirata K, John ER, Prichep L, Biscay-Lirio R, Kinoshita T. Assessing interactions in the brain with exact low-resolution electromagnetic tomography. Philos Trans R Soc Math Phys Eng Sci. 2011; 369:3768–3784.

Pine DS, Cohen P, Gurley D, Brook J, Ma Y. The risk for early-adulthood anxiety and depressive disorders in adolescents with anxiety and depressive disorders. Arch Gen Psychiatry. 1998; 55:56–64. [PubMed: 9435761]

Pontifex MB, Scudder MR, Brown ML, O'Leary KC, Wu C-T, Themanson JR, Hillman CH. On the number of trials necessary for stabilization of error-related brain activity across the life span. Psychophysiology. 2010; 47:767–773. [PubMed: 20230502]

Reynolds GD, Richards JE. Cortical Source Localization of Infant Cognition. Dev Neuropsychol. 2009; 34:312–329. [PubMed: 19437206]

Richards JE. Cortical sources of ERP in prosaccade and antisaccade eye movements using realistic source models. Front Syst Neurosci. 2013:7. [PubMed: 23596400]

Richards JE, Boswell C, Stevens M, Vendemia JMC. Evaluating Methods for Constructing Average High-Density Electrode Positions. Brain Topogr. 2015; 28:70–86. [PubMed: 25234713]

Richards JE, Sanchez C, Phillips-Meek M, Xie W. A database of age-appropriate average MRI templates. NeuroImage. 2016; 124:1254–1259. [PubMed: 25941089]

Richards, JE., Xie, W. Advances in Child Development and Behavior. Elsevier; 2015. Brains for All the Ages; p. 1-52.

Rorden, CR. MRIcroGL. McCausland Center; 2012. Available at: http://www.mccauslandcenter.sc.edu/mricrogl/

Santesso DL, Segalowitz SJ. Developmental differences in error-related ERPs in middle- to late-adolescent males. Dev Psychol. 2008; 44:205–217. [PubMed: 18194018]

Seeley WW, Menon V, Schatzberg AF, Keller J, Glover GH, Kenna H, Reiss AL, Greicius MD. Dissociable Intrinsic Connectivity Networks for Salience Processing and Executive Control. J Neurosci. 2007; 27:2349–2356. [PubMed: 17329432]

Shattuck DW, Mirza M, Adisetiyo V, Hojatkashani C, Salamon G, Narr KL, Poldrack RA, Bilder RM, Toga AW. Construction of a 3D probabilistic atlas of human cortical structures. NeuroImage. 2008; 39:1064–1080. [PubMed: 18037310]

Shenhav A, Botvinick MM, Cohen JD. The Expected Value of Control: An Integrative Theory of Anterior Cingulate Cortex Function. Neuron. 2013; 79:217–240. [PubMed: 23889930]

Somerville LH, Casey B. Developmental neurobiology of cognitive control and motivational systems. Curr Opin Neurobiol. 2010; 20:236–241. [PubMed: 20167473]

Sowell ER, Thompson PM, Holmes CJ, Batth R, Jernigan TL, Toga AW. Localizing Age-Related Changes in Brain Structure between Childhood and Adolescence Using Statistical Parametric Mapping. NeuroImage. 1999a; 9:587–597. [PubMed: 10334902]

Sowell ER, Thompson PM, Holmes CJ, Jernigan TL, Toga AW. In vivo evidence for post-adolescent brain maturation in frontal and striatal regions. Nat Neurosci. 1999b; 2:859–861. [PubMed: 10491602]

Steele VR, Anderson NE, Claus ED, Bernat EM, Rao V, Assaf M, Pearlson GD, Calhoun VD, Kiehl KA. Neuroimaging measures of error-processing: Extracting reliable signals from event-related potentials and functional magnetic resonance imaging. NeuroImage. 2016; 132:247–260. [PubMed: 26908319]

Swick D, Ashley V, Turken AU. Left inferior frontal gyrus is critical for response inhibition. BMC Neurosci. 2008; 9:102. [PubMed: 18939997]

Tamnes CK, Østby Y, Fjell AM, Westlye LT, Due-Tønnessen P, Walhovd KB. Brain Maturation in Adolescence and Young Adulthood: Regional Age-Related Changes in Cortical Thickness and White Matter Volume and Microstructure. Cereb Cortex. 2010; 20:534–548. [PubMed: 19520764]

Tamnes CK, Walhovd KB, Torstveit M, Sells VT, Fjell AM. Performance monitoring in children and adolescents: A review of developmental changes in the error-related negativity and brain maturation. Dev Cogn Neurosci. 2013; 6:1–13. [PubMed: 23777674]

Taylor SF, Stern ER, Gehring WJ. Neural systems for error monitoring recent findings and theoretical perspectives. The Neuroscientist. 2007; 13:160–172. [PubMed: 17404376]

Ullsperger M, Danielmeier C, Jocham G. Neurophysiology of Performance Monitoring and Adaptive Behavior. Physiol Rev. 2014; 94:35–79. [PubMed: 24382883]

Van Veen V, Carter CS. Error Detection, Correction, and Prevention in the Brain: A Brief Review of Data and Theories. Clin EEG Neurosci. 2006; 37:330–335. [PubMed: 17073172]

Vorwerk J, Cho J-H, Rampp S, Hamer H, Knösche TR, Wolters CH. A guideline for head volume conductor modeling in EEG and MEG. NeuroImage. 2014; 100:590–607. [PubMed: 24971512]

Weinberg A, Meyer A, Hale-Rude E, Perlman G, Kotov R, Klein DN, Hajcak G. Error-related negativity (ERN) and sustained threat: Conceptual framework and empirical evaluation in an adolescent sample. Psychophysiology. 2016; 53:372. [PubMed: 26877129]

Westlye LT, Walhovd KB, Bjørnerud A, Due-Tønnessen P, Fjell AM. Error-Related Negativity is Mediated by Fractional Anisotropy in the Posterior Cingulate Gyrus—A Study Combining Diffusion Tensor Imaging and Electrophysiology in Healthy Adults. Cereb Cortex. 2009; 19:293–304. [PubMed: 18502729]

Highlights

- ERN topography and source activity changed as a function of age (9–35 years)

- Two primary clusters of neural activity found to give rise to the ERN

- Dorsal cluster stable across age, ventral-frontal cluster increased with age

- Dorsal cluster (including posterior cingulate) predicted control after errors

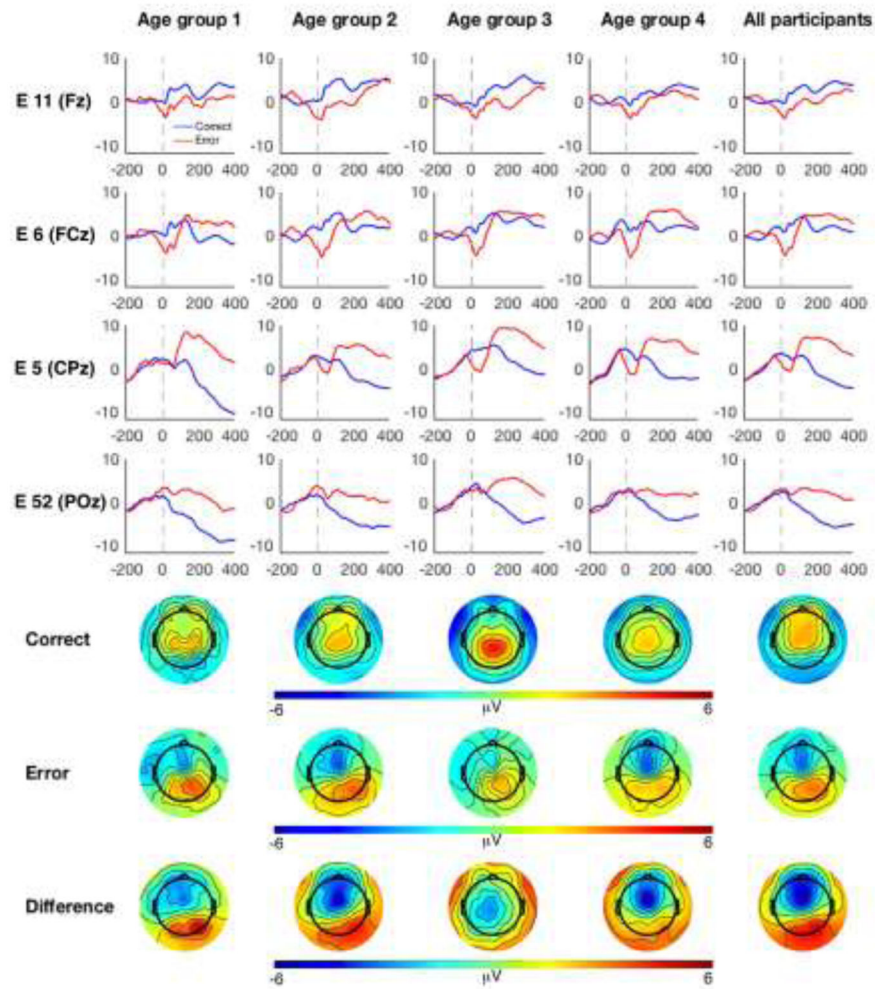- Data serve as model of typical error-monitoring development

Figure 1.
ERP and topographic plots as a function of age. The first four rows correspond to EGI electrode locations along the midline. For display purposes, ERPs and related scalp topographies are plotted as four separate age groups (first four columns) in addition to the grand average (fifth column). ERPs are plotted relative to response onset; correct responses are plotted in blue and incorrect responses are plotted in red. Topographic plots reflect mean amplitude during a 40 ms window centered on each individual's peak of the ERN and CRN.
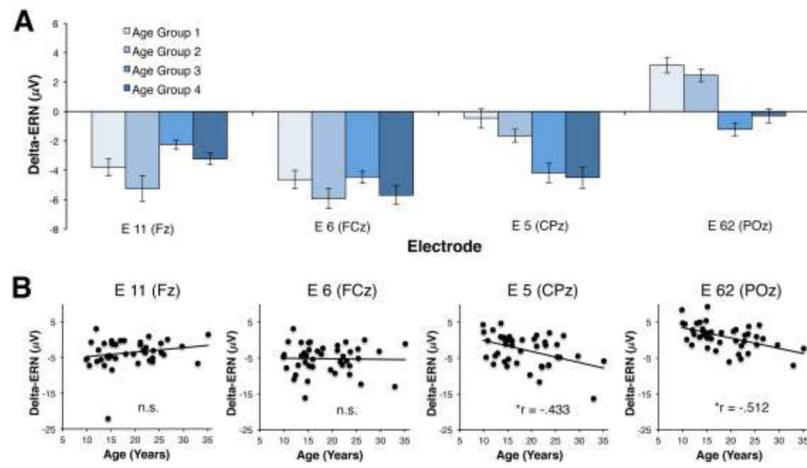
Figure 2.
Age related changes in ERP activity. (A) For display purposes, ERN-CRN (delta-ERN) activity is plotted for the four separate age groups. Bar plots reflect mean amplitude of the delta-ERN at four midline EGI electrode locations. (B) Scatterplots depicting the relationship between delta-ERN and age at the four separate midline electrode locations. Note: * denotes a significant effect following correction for multiple comparisons; n.s. = "non-significant".
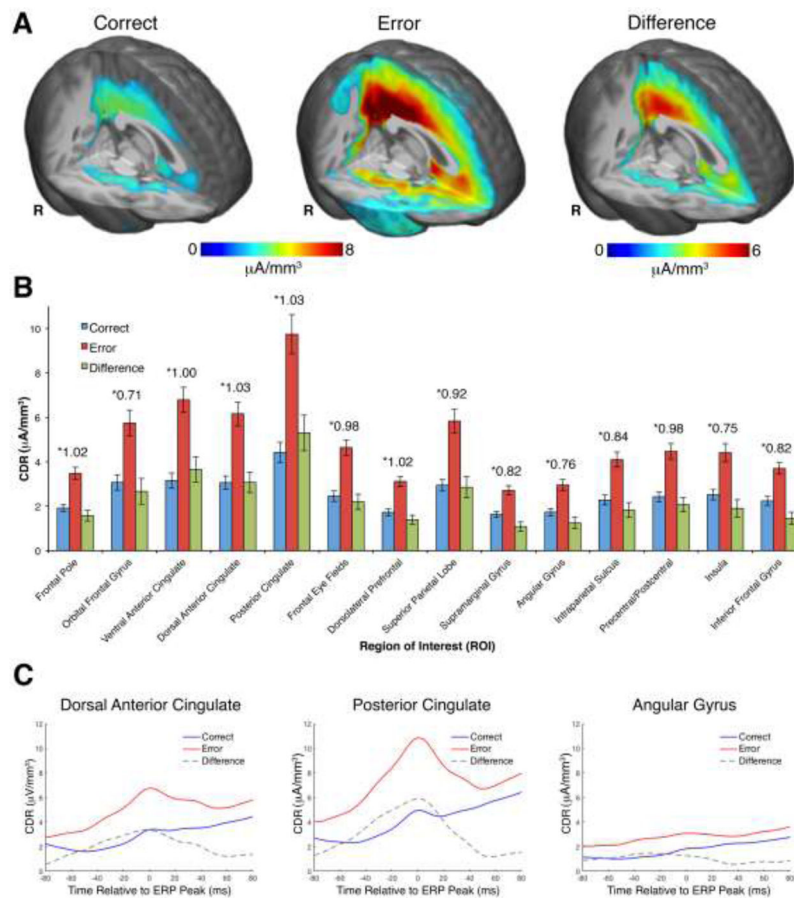
Figure 3.
Source localization of the ERN and CRN. (A) 3D renderings of the current density reconstruction (CDR) for correct and error responses. For display purposes, the correct CDR was also subtracted from the error CDR and plotted as a 3D rendering (labeled "difference"). Correct and error CDR renderings are thresholded at 2.5 µA/mm3, whereas the error-correct CDR rendering is thresholded at 2 µA/mm3. (B) CDR activity for correct and incorrect responses extracted from 14 regions of interest (ROIs); the error-correct difference is also plotted. Effect sizes (Cohen's *d*) for the correct/incorrect comparison within each ROI are indicated with asterisks; error bars reflect standard error of the mean. (C) Time course of CDR activity in three exemplar ROIs, centered on the peak of the ERN and CRN.
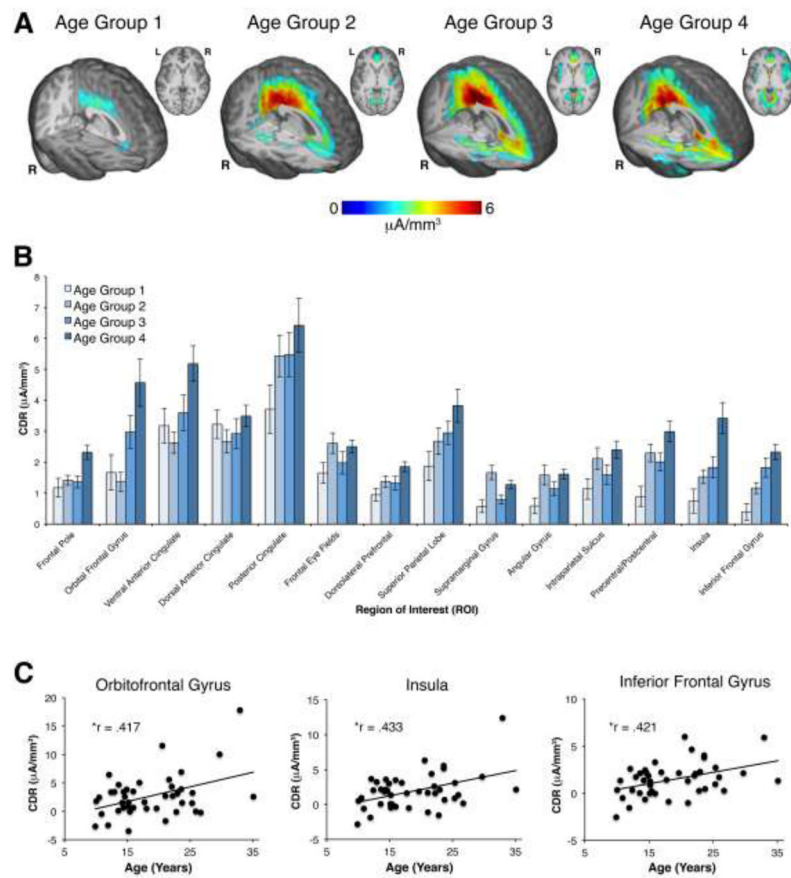
Figure 4.
Age-related changes in ERN/CRN source activity. (A) For display purposes the correct CDR was subtracted from the error CDR and plotted as four separate age groups; error-correct CDR activity is rendered for each age group on an age-appropriate MRI template. CDR renderings are thresholded at 2 μA/mm3.(B) Error-correct CDR activity is plotted for the four age groups, for all 14 regions of interest (ROIs). (C) Scatterplots depicting the three ROIs in which a significant relationship between age and CDR activity were identified. Note: * denotes a significant effect following correction for multiple comparisons.
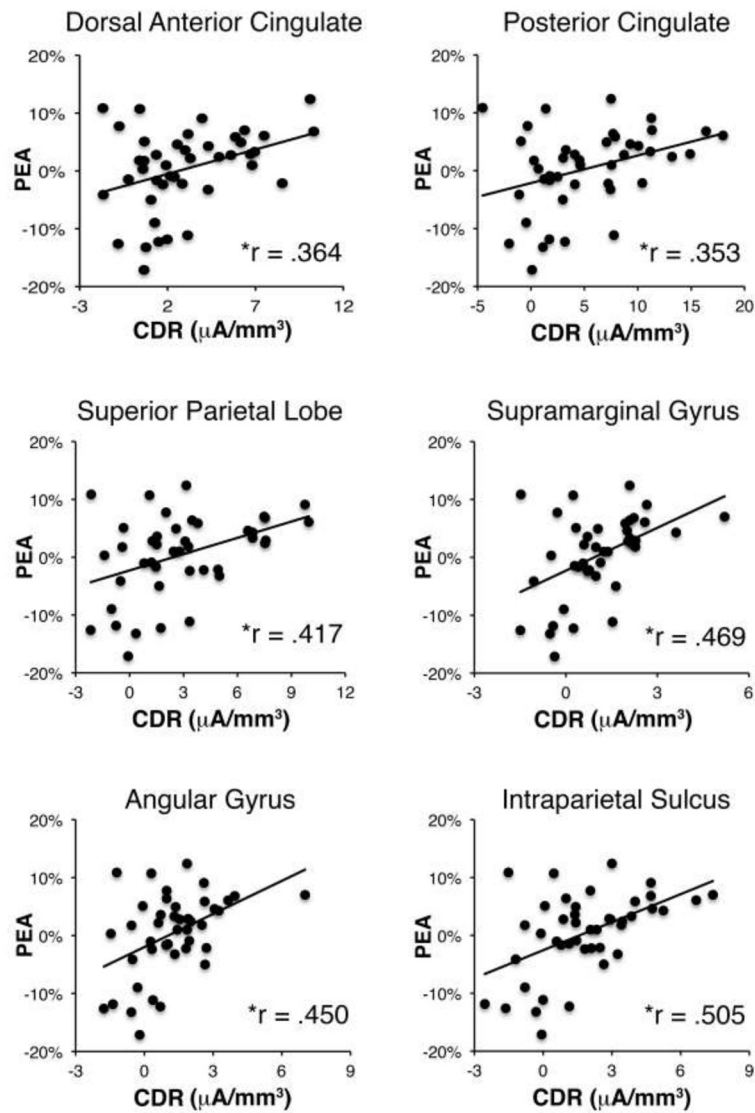
Figure 5.
Relations between CDR activity and post-error accuracy. Scatterplots depicting the six ROIs in which a significant relation between CDR activity and post-error accuracy (PEA) was identified. Note: * denotes a significant effect following correction for multiple comparisons.

Table 1

Description of the atlas locations used to define each region of interest (ROI) that was used for the analysis of the current density reconstruction (CDR) data. Numbers correspond to anatomical locations in the respective atlases.

Regions of interest for the analysis of CDR data		
Inferior frontal gyrus (bi-lateral)		
LPBA40:	25, 26	Inferior frontal gyrus (L,R)
Hammers:	56, 57	Inferior frontal gyrus (L,R)
Brodman:	47	Inferior frontal gyrus
Insula (bi-lateral)		
Lobar:		Insula
LBPA40:	101,102	Insular cortex (L,R)
Hammers:	20,21	Insula (L,R)
Dorsolateral prefrontal cortex (bi-lateral)		
Brodmann:	9, 46	Dorsolateral prefrontal cortex
Frontal eye fields (bi-lateral)		
Brodmann:	6, 8	Premotor, frontal eye fields
Precentral and postcentral gyrus (bi-latereal)		
LPBA40:	27,28	Precentral gyrus (L,R)
	41,42	Postcentral gyrus (L,R)
Hammers:	50,51	Precentral gyrus (L,R)
	60,61	Postcentral gyrus (L,R)
Superior parietal lobe (bi-latereal)		
LPBA40:	43,44	Superior parietal gyrus(L,R)
Hammers:	62,63	Superior parietal gyrus(L,R)
Supramarginal gyrus (bi-lateral)		
LPBA40:	45,46	Supramarginal gyrus (L,R)
Angular gyrus (bi-lateral)		
LPBA40:	47,47	Angular gyrus
Intraparietal sulcus (bi-lateral)		
3mm border between inferior parietal lobe (LPBA40 SMG, AG; Hammers Remainder of parietal cortex) and superior parietal lobe (LPBA40 and Hammers)		
Frontal pole		
Harvard- Oxford:		Frontal pole
Orbito-frontal gyrus		
LPBA40:	29,30	Middle orbitofrontal gyrus
	33,34	Gyrus rectus
Hammers:	53, 53	Straight gyrus
	68,69	Medial orbital gyrus
Ventral anterior cingulate cortex		
(Anterior to AC, superior to mid-corpus callosum)		
LPBA40:	121,122	Cingulate gyrus
Hammers:	76,77	Subgenual anterior cingulate

Regions of interest for the analysis of CDR data		
	78,79	Subcallosal area
	80,81	Pre-subgenual anterior cingulate
	24,25	Cingulate gyrus, anterior (supragenual)
Harvard- Oxford		Paracingulate gyrus
Dorsal anterior cingulate cortex		
(Anterior to AC, superior to mid-corpus callosum)		
LPBA40	121,122	Cingulate gyrus
Hammers	24,24	Cingulate gyrus,anterior (supragenual)
Posterior cingulate cortex		
(Posterior to AC)		
LBPA40:	121,122	Cingulate gyrus
Hammers:	26, 27	Cingulate gyrus, posterior part

Note. AC anterior commisure, CDR current density reconstruction, SMG supramarginal gyrus

Table 2

Partial correlation coefficients for the relation between current density reconstruction (CDR) activity within each of the 14 regions of interest (ROIs) and either age, post-error accuracy (PEA), or post-error slowing (PES), when controlling for sex. Partial correlation coefficients for the relation between CDR activity within each of the 14 ROIs and PEA, when controlling for both sex and age, are also displayed.

Correlations between age, behavior, and neural activity

Control variable	FP	OFC	vACC	dACC	PCC	FEF	DLPFC	sPL	SMG	AG	IPS	CG	Insula	IFG
Age	.29	.417*	.258	.053	.165	.085	.2	.199	.097	.15	.119	.302	.433*	.421*
PEA	.27	.17	.26	.364*	.353*	.317	0.336	.417*	.469*	.45*	.505*	.3	.283	.231
PES	.127	.099	.095	−.014	.002	−.066	.092	.073	.102	.025	.089	.055	.101	.102
Age PEA	.296	.208	.281	.367*	.366*	.322	.352*	.435*	.476*	.462*	.514*	.328	.335	.275